Length Variation Effect of the Impulse Response Model of a Secondary Path in Embedded Control

Hamid[1]
Department of Computer Science, University of Kashmir,Hazratbal,Srinagar

Research Article

Date of Submission: 17-02-2025 **Date of Acceptance: 15-04-2025** **Date of Publication: 27-05-2025**

ABSTRACT

The length variation impact of the impulse response function (IRF) for the secondary path model in active noise control utilizing an embedded control board is investigated theoretically and experimentally in this work. The control disturbance in an 1800 mm-long duct was a narrowband sweep noise. The length variation of the IRF model integrated into an adaptive feedforward filtered-x LMS (FxLMS) method was then examined in terms of the mean square error, computation cost, stability requirement, and attenuation performance before and after control. A dSPACE DS1104 embedded control board was used to build the FxLMS algorithm with different IRF lengths for real-time control. Ultimately, the systematic analysis can find the most suitable IRF length, taking into account computing complexity and performance. The study's findings can be used to realistic active noise control systems.

Introduction

A technology based on adaptive feedforward control, active noise cancellation (ANC) is primarily used to superimpose an artificial sound over an undesired disturbance noise [1-3]. For optimal performance, the fake sound produced by the secondary loudspeaker must have the same loudness but be precisely antiphase to the source noise. When using the filtered-x least mean square (FxLMS) method, an ANC system needs a suitable model for the compensation of the secondary route (or the plant). The performance, stability, and convergence speed of the ANC system are known to be significantly impacted by both the convergence coefficient and the correctness of the secondary path model [1, 4]. Because the FIR filter is reliable and simple to construct, the impulse response function (IRF) of the secondary route of the FxLMS technique is often implemented as a FIR (finite impulse response) filter in a real-time embedded control board. To reduce the amount of computing required, a lengthy FIR filter may be replaced with an IIR (infinite impulse response) filter, albeit the IIR filter is more prone to instability than a FIR filter.

In terms of computing complexity, control stability, and performance, an ideal IRF length is crucial. The primary acoustic modes that need to be suppressed or managed in the secondary route must be contained within the ideal IRF length. The plant's uncertainty results from the discrepancy between the intended IRF and the actual secondary route [1, 5]. When the plant is disturbed, this discrepancy increases. For the FxLMS algorithm to be stable and function well, the secondary path's IRF length is thus crucial.

Ren and Kumar proposed an SPR (strictly positive real) criterion for the FxLMS algorithm's robust stability by integrating the secondary route and its model [6]. Fraanje et al. looked at minimal norm regularization filters that may stabilize the update algorithm to avoid instability since an unstable update technique might deteriorate the program's performance in addition to the uncertainty of the plant model [7]. Without measuring the plant uncertainty, Berkhoff investigated a method for enhancing the stability of adaptive feedforward controllers [8].

In this work, the control performance is analyzed by taking into account the length fluctuation of the IRF of the secondary

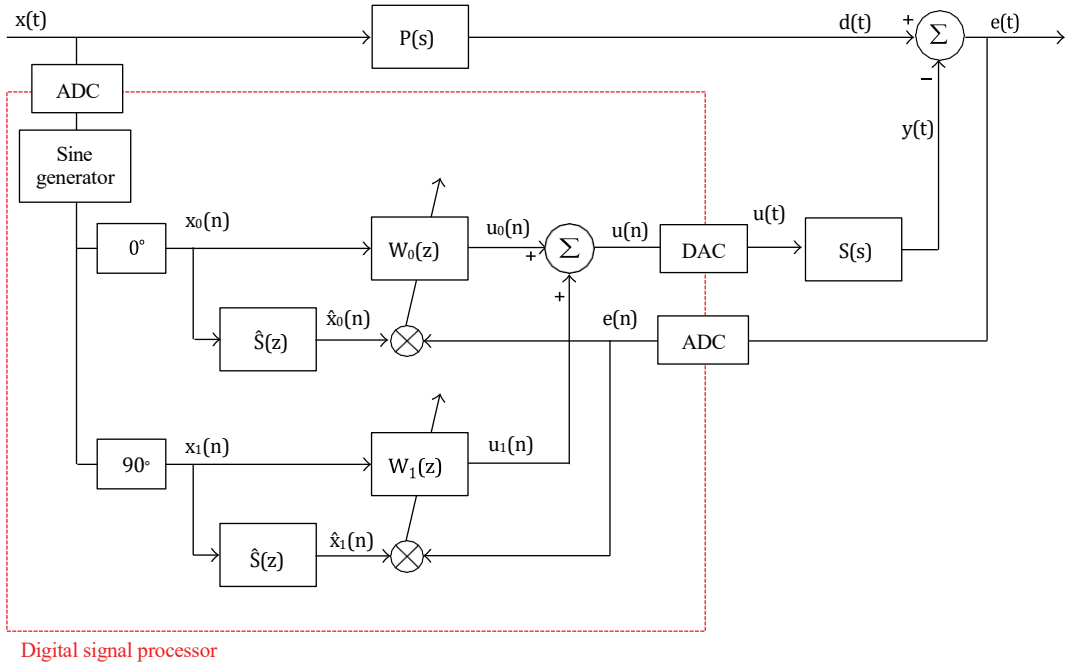


FIGURE 1: Block diagram of the narrowband FxLMS algorithm.

stability, and the computation complexity for a duct ANC system and an optimum IRF length is determined.

In Section 2, a theoretical examination is investigated for the effect of the IRF of the secondary path in the FxLMS algorithm. Section 3 shows the experimental setup for real- time ANC control of the duct system. Section 4 includes the results and analysis of the control experiment. Finally conclusions are described in Section 5.

1. Theoretical Considerations

Figure 1 shows a typical ANC block diagram of the SISO (single input single output) adaptive feedforward FxLMS algorithm that cancels the primary narrowband noise by the secondary source [1].

As illustrated in Figure 1, $x(t)$ is the reference signal, $d(t)$ is the disturbance signal, $u(t)$ is the control effort, $y(t)$ is the plant output and $e(t)$ is the error signal, and $P(s)$ and $S(s)$ are the primary and secondary paths, respectively. The blocks inside the rectangle with red dashed line are implemented in a DSP (digital signal processor) where $W(z)$ and $\hat{S}(z)$ are the adaptive filter and the IRF of the secondary path model, respectively. In addition $x(n)$, $\hat{x}(n)$, $u(n)$, and $e(n)$ are discrete signals to represent the reference, filtered reference, control effort, and error sequences, respectively.

Assuming 1 reference signal, 1 primary loudspeaker, 1 secondary loudspeaker, and 1 error microphone are installed in a duct system, the filtered reference sequence $\hat{x}(n)$ can be expressed as

$$\hat{\mathbf{x}}_i(n) = \hat{\mathbf{s}}^T \mathbf{x}_i(n-\ell), \qquad (i = 0, 1,\ \ell = 0 \sim L-1), \qquad (1)$$

where L is the IRF filter length of $\hat{S}(z)$ and $\hat{\mathbf{s}}$ is the coefficient of the IRF filter. The update equation of an adaptive feedforward narrowband FxLMS algorithm can be written by [1–4]

$$\mathbf{w}_i(n+1) = \mathbf{w}_i(n) + \alpha \hat{\mathbf{x}}_i(n)\, e(n), \qquad (2)$$

where α is the convergence coefficient. The computation to obtain the control effort $u(n)$ in the DSP can be given by

$$u(n) = w_0(n)\, x_0(n) + w_1(n)\, x_1(n). \qquad (3)$$

Provided that $\hat{S}(z)$ is approximately identical to $S(z)$, the cancellation of the primary noise can be achieved during con- trol as the IRF of the secondary path model can compensate

for the actual secondary path. However, the IRF with some error makes a certain level of residual noise during control as

$$e(t) = d(t) - y(t) \neq 0. \quad (4)$$

Thus the accuracy of the IRF modeling of the secondary path is critically important in the implementation of an FxLMS based ANC system.

The computation complexity of the SISO FxLMS algo- rithm by length variation of the IRF filter can be given by Table 1, where the IRF filter length and control order number are L and C, respectively.

2. Experimental Setup

The experimental setup for the narrowband SISO ANC control is displayed in Figure 2. A duct (length = 1800 mm) ANC system is comprised of a primary loudspeaker at

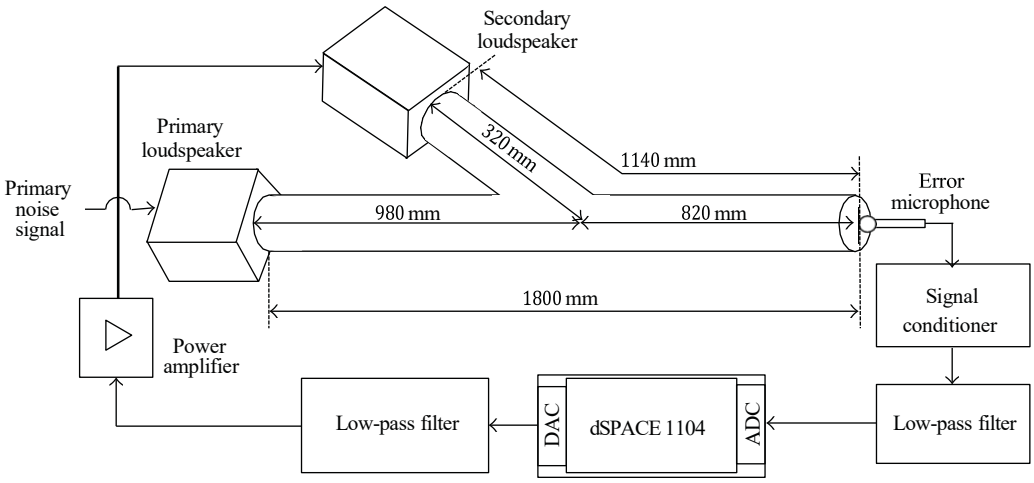


FIGURE 2: Experimental setup for the narrowband ANC for a duct.

TABLE 1: Computation complexity of the narrowband FxLMS algorithm.

Equation	Number of additions	Number of multiplications
(1)	$2(L-1)C$	$2LC$
(2)	$2C$	$2C+1$
(3)	$2C-1$	$2C$
Total	$2C(L+1)-1$	$2C(L+2)+1$

the left end, a secondary source (control loudspeaker), an error microphone (1/2 PCB 377B11) at the right end, a power amplifier (B&K 2716C), a PCB signal conditioner, two low- pass filters (cutoff frequency: f_c = 500 Hz), and a dSPACE 1104 controller for the implementation of the SISO FxLMS
algorithm.

The primary disturbance was a narrowband signal with some sinusoidal waves such as a powertrain interior noise of a passenger car. In this study, the largest four orders by the powertrain of the passenger car are the primary noise. The primary and secondary paths were measured at first and, after carrying out the offiine modeling of the secondary path, the IRF model with various lengths was calculated and implemented in the control board. Then the real-time ANC control experiment was accomplished with each IRF model.

3. Results and Discussions

3.1. IRF Modeling from the Measured Secondary Path. White noise was used to measure the secondary path (secondary loudspeaker-error microphone) response when the sam- pling frequency was f_s = 6,000 Hz. The sampling frequency was maintained the same all the time during this study.

Figure 3(a) demonstrates that the IRF model from the mea- sured secondary path response of the duct system has two peaks

at 25 and 55 samples, respectively, and then decays quickly after 100 samples. The first and second peaks at the sample of 25 and 55, respectively, are the most important contributions to the IRF and indicate the time delays in the secondary path of about 4.17 msec and 9.17 msec, respec- tively. As can be seen from Figure 3(a), at the sample of 400, the IRF settles down on zero and this allows assuming that the IRF length of 400 samples may represent the secondary path response accurately. Thus the digital plant model with
the IRF length of $L = 400$, $\hat{S}_{400}(z)$, can be an approximated model of the actual plant (secondary path), $S(z)$, as follows:

$$\hat{S}_{400}(z) \approx S(z). \quad (5)$$

Four different IRF lengths of $L = 30$, 63, 93, and 400 are considered and plotted in Figure 3(b) to compare their frequency response functions (FRFs). The magnitude of the FRF with $L = 30$ (dashed lines) traces simply the averaged plot
of the FRF with $L = 400$ (thick solid lines) without resonances
or antiresonances in the frequency range below 1200 Hz and its phase response looks almost as a straight line. For $L = 63$, the magnitude response follows some main resonances and antiresonances as shown in Figure 3(b). In the case of $L = 93$, the magnitude and phase responses are very similar to those of $L = 400$.

The mean square error (MSE) is defined by the difference
between the two plant models of $\hat{S}_{400}(z)$ and $\hat{S}_L(z)$ when the input signal $x(n)$ is a white noise and can be represented as

$$\text{MSE} = E[x(n)[\hat{S}_{400}(z) - \hat{S}_L(z)]], \quad (6)$$

where $E[\,]$ is the expectation operator. As the MSE indicates the accuracy of the secondary path model by comparing the outputs of the actual secondary path and its model against a
white noise input, the MSE is an important factor to assess the model reliability.

The MSE curve against the IRF length of $L = 0$–120 is plotted in Figure 4(a) and it indicates that the MSE is dramatically reduced by the increase of the IRF length.
Actually the inclusion of the peaks in the IRF of Figure 4(a) gives the most critical influences to the accuracy of modeling of the secondary path. For the best performance and robust stability, every peak is necessary in the IRF model; however

FRF of the secondary path in Figure 3(b) and two valleys between them at about 270–320 and 460–530 Hz. In case of $L = 30$, the frequency ranges for the peaks and valleys are partially different. The frequencies of the valleys such as around 300 Hz and 500 Hz in Figure 7 are almost identically
located to the unattenuated frequencies as can be seen from Figure 6.

This coincidence discloses maintaining as higher values of $\text{Re}[S(e^{j\omega T})\hat{S}_L(e^{j\omega T})]$ as possible in the frequency range of interest and this allows higher convergence coefficients
to achieve further attenuation. The valleys near zero in Figure 7 strictly restrict the increase of the convergence

the reduction; however the reduction difference between the IRF lengths of $L = 63$ and 93 samples is not clearly distinguished. The largest reduction achieved about 25–40 dB at 100–250 Hz when both $L = 63$ and 93, but the reduction at $L = 30$ was 5–10 dB smaller than them as illustrated in Figure 6(b).

3.2. Comparison of Robust Stability by IRF Length Variation. It is noted from Figure 6(b) that the attenuations at some frequency ranges, such as about 100–120, 300–350, and 480–500 Hz, are not attained properly compared to other frequencies. This suggests that, in these frequency ranges, the control stability could be easily collapsed if the convergence coefficient is increased by even a small value to achieve further attenuation. This is basically caused by the acoustical properties of the duct and can be additionally explained by the primary and secondary paths.

It is known that the stability requirement for the FxLMS algorithm can be expressed by [1, 5, 6]

$$\text{Re}[S(e^{j\omega T})\hat{S}_L(e^{j\omega T})] > 0, \quad \forall \omega T, \quad (7)$$

3.3. Comparison of Computation Complexity by IRF Length Variation. Computation complexity defined in Table 1 against various IRF lengths with the FxLMS algorithm their mean values of attenuation in the duct ANC experiment are summarized in Table 2. The IRF lengths considered in
the control experiment are $L = 30$, 54, 63, 70, 80, 86, 93, 99, and 400. Table 2 shows the attenuation is almost the same of about -21.50 dB in average when L is greater than or equal to 63. Considering the computation complexity and
performance by the IRF length variation, it indicates that the IRF length of $L = 63$, which contains the two major peaks in the IRF graph as plotted in Figure 3(a), is the most reasonable choice in the duct system. This analysis allows relieving the computation complexity by reducing about 84% of the IRF length with the same performance as presented in Table 2.

Therefore, the IRF length variation effect of the secondary path model $\hat{S}_L(z)$ is investigated in this study in terms of MSE, involvement of major peaks in the IRF graph, stability
requirement, and attenuation and these terms have strong correlations with the optimum IRF length. The results in this study can be useful in various ANC applications.

In case the primary noise is broadband, it is expected that this approach can be worked well since it is based on the

where ω is the frequency and T is the sampling interval. The stability requirement over frequency in (7) is satisfied with three different IRF lengths of $L = 63$ (thick solid line), 93 (thin solid line), or 400 (dashed line) as presented in Figure 7.

But, in the case of $L = 30$ (dashed and dotted line), the requirement is unsatisfied at the frequencies below 100 Hz and this implies the FxLMS control with $L = 30$ can cause instability if the control frequency range involves below 100 Hz. Thus the stability requirement in (7) must be considered in the determination of the IRF length in advance of control.

Figure 7 displays three outstanding peaks, assuming that $\mathrm{Re}[S(e^{j\omega T})\hat{S}_L(e^{j\omega T})] > 0.2$, at about 100–270, 320–460, and 530–600 Hz are the three largest resonant frequencies of the analysis of the secondary path.

IRF length (L)	Number of additions	Number of multiplications	Mean value of attenuation [100~500 Hz]
30	247 (7.70%)	257 (7.99%)	−15.01 dB
54	439 (13.69%)	449 (13.96%)	−20.78 dB
63	**511 (15.93%)**	**521 (16.20%)**	**−21.48 dB**
70	567 (17.68%)	577 (17.94%)	−21.57 dB
80	647 (20.17%)	657 (20.42%)	−21.37 dB
86	695 (21.67%)	705 (21.91%)	−21.63 dB
93	751 (23.42%)	761 (23.66%)	−21.21 dB
99	799 (24.91%)	809 (25.15%)	−21.37 dB
400	3207 (100%)	3217 (100%)	—

TABLE 2: Computational complexity per sample and mean values of attenuation by the IRF length variation ($\alpha = 0.01$).

4. Conclusions

This study presents the length variation effect of the sec- ondary path IRF model in an ANC duct system. The main investigations can be described in the following.

The major peaks in the full IRF graph are needed to be involved in the IRF model for the FxLMS algorithm. Although the computation complexity is limited, the IRF model requires containing the peakiest and the next samples at least of the last major peak in the full IRF graph. The stability requirement of $\mathrm{Re}[S(e^{j\omega T})\hat{S}_L(e^{j\omega T})] > 0$ must be considered in the determination of the IRF length in advance of control. In addition, robust stability with higher performance demands higher values of $\mathrm{Re}[S(e^{j\omega T})\hat{S}_L(e^{j\omega T})]$ at the valleys in the frequency ranges of interest.

This investigation clarifies that the most reasonable IRF length, considering the computation complexity and performance, for the implementation in an embedded control board can be determined systematically through the investigation on an ANC duct system in this study. For future study, this approach will be extended to an ANC system against a broadband primary noise.

References

[1] S. J. Elliott, *Signal Processing for Active Control*, Academic Press, New York, NY, USA, 2001.

[2] K. Lee, W. S. Gan, and S. M. Kuo, *Subband Adaptive Filtering: Theory and Implementation*, John Wiley & Sons, 2009.

[3] Y. Kajikawa, W.-S. Gan, and S. M. Kuo, "Recent advances on active noise control: open issues and innovative applications," *APSIPA Transactions on Signal and Information Processing*, vol. 1, article e3, 2012.

[4] S. Ryu, Y. J. Park, and Y.-S. Lee, "Active suppression of narrow- band noise by multiple secondary sources," *Journal of Sensors*, vol. 2016, Article ID 6276828, 9 pages, 2016.

[5] M. Morari and E. Zafiriou, *Robust Process Control*, Prentice- Hall, London, UK, 1989.

[6] W. Ren and P. R. Kumar, "Adaptive active noise control: structures, algorithms and convergence analysis," in *Proceedings of the Engineering for Environmental Noise Control (Inter-Noise '89)*, pp. 435–440, Newport Beach, Calif, USA, November 1989.

[7] P. R. Fraanje, S. J. Elliott, and M. Verhaegen, "Robustness of the filtered-X LMS algorithm—part II: robustness enhancement by minimal regularization for norm bounded uncertainty," *IEEE Transactions on Signal Processing*, vol. 55, no. 8, pp. 4038–4047, 2007.

[8] A. P. Berkhoff, "A technique for improved stability of adaptive feedforward controllers without detailed uncertainty measure- ments," *Smart Materials and Structures*, vol. 21, no. 6, Article ID 064003, 2012.